New Method Determines Optimized Reference SDM for MIMO Testing

Marcos A. Underwood, Ph.D.
Tu'tuli Enterprises and
MSI DFAT Chief Scientist

Abstract: The paper presents a new method for vibration testing of articles such as satellites, aerospace subsystems, transportation subsystems, civil structures, or articles whose reliability in operation may be evaluated using either mechanical or acoustic vibration testing. The method can be used for direct field or reverberant acoustic test facility testing (acoustic) systems or multiple-exciter (mechanical) testing systems to perform vibration testing. The method improves the ability of Multiple-Input-Multiple-Output (MIMO) acoustic testing systems to create diffuse or other types of acoustic fields and MIMO mechanical testing systems to produce vibration responses conforming to an initial reference Spectral Density Matrix (SDM) specification in the least mean-square error (LMSE) sense. It provides an updated positive definite or semi-definite reference SDM that enables such tests to run with less error, using minimum required drive power, as a function of the initial definition of the reference SDM, by modifying its coherence and phase off-diagonal terms, to approximate initially defined off-diagonal terms in the LMSE sense, but maintaining its initially defined diagonal terms exactly, while accounting for physical limitations existing in the overall MIMO testing system.

Introduction

For Direct Field Acoustic Testing (DFAT™) [4,5], Reverberant Acoustic Test Facility (RATF) Testing [1], and Multi-exciter Vibration Testing [17,18,22,23] it is desirable to control numerous parameters of the acoustic response field or the response vibrations due to the excitation from multiple actuators according to a predetermined reference Spectral Density Matrix (SDM) [17,20,22,23,24,26,29] Reference specification.

Test results will be presented in later sections showing the benefits of the new method that were obtained by the Multiple-Input-Multiple-Output (MIMO) acoustic control system described by the block diagrams shown in Fig. 1 and by the MIMO vibration control system described in Fig. 2. The most notable difference between these block diagrams and those employed by other MIMO control systems, is the use of the author's patented MIMO adaptive control method [14,15,16], which is based on modern optimal control, and which is shown by the "correct drive SDM" and "Cholesky decomposition" blocks in Figs. 1 and 2. The adaptive optimal control method used within these blocks performs a multi-dimensional control optimization each control-loop iteration, which leads to a drive SDM requiring the least power and which produces the least mean-squared control-error, restricted only by limitations in the system-under-test and the definition of the predetermined reference SDM. The main difference between Fig. 1 and 2 is the absence of the n^{th} octave conversion and n^{th} octave reference in Fig. 2 and their respective fields of applicability, e.g. the need to address the inherent delays and reverberation in acoustics.

In a typical MIMO acoustic control system, as illustrated by Fig. 1 and discussed in [4-6,26,27,29], a reference SDM is typically provided that contains the desired predetermined acoustic field parameters. During operation the system will make adjustments to the drive signals for multiple groups of independently controllable transducers so that the resulting acoustic field will match the predetermined acoustic field specifications contained in the reference SDM as closely as possible. However, the predetermined acoustic field specifications typically ignore the real-world constraints of the testing system, its components and the facility itself [27]. As a result, during operation, adjustments to the drive signals, may fail to yield an acceptable acoustic response and may exceed the capabilities of the acoustic test system leading to self-limiting by components of the system with the potential for damage to the system components or the test article itself.

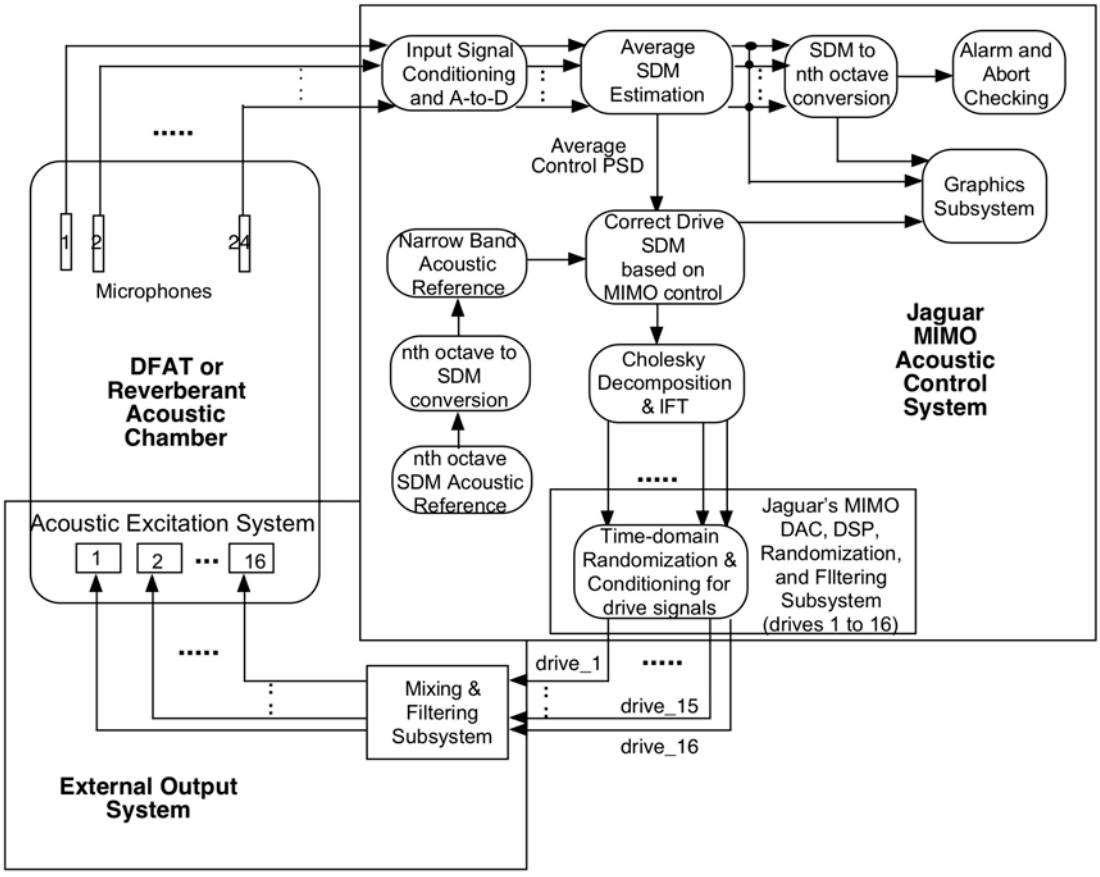

Fig. 1: MIMO Acoustic Control System

Similarly, for multi-exciter mechanical vibration testing (where an exciter can either be an electro-hydraulic actuator, electro-dynamic shaker, ceramic shaker, or collections of such vibration transducers) [13-19,22-24,29], it is also desirable to control numerous parameters of the multi-exciter vibration test according to a predetermined specification [7,8,12-15,17-19,22-24,29]. In a typical MIMO multi-exciter vibration test control system, as described in [13,14,15,17,19,22,23,29] and illustrated by Fig. 2, a reference SDM is also typically provided that contains the desired predetermined multi-exciter vibration test parameters.

During operation the MIMO mechanical vibration control system, will adjust the drive signals for multiple groups of separately controllable exciters so that the resulting multi-exciter mechanical vibration test responses will match the predetermined multi-exciter mechanical vibration test specifications contained in the reference as closely as possible [13,17,18,19,22-24]. However, the predetermined multi-exciter mechanical vibration test specifications also typically ignore the real-world constraints of the test system and its components [27]. As a result, during operation, adjustments to the drive signals may also exceed the capabilities of the mechanical vibration test system leading to self-limiting by components of the test system, failure to meet the specified test parameters, and possible damage to the system components or the test article itself.

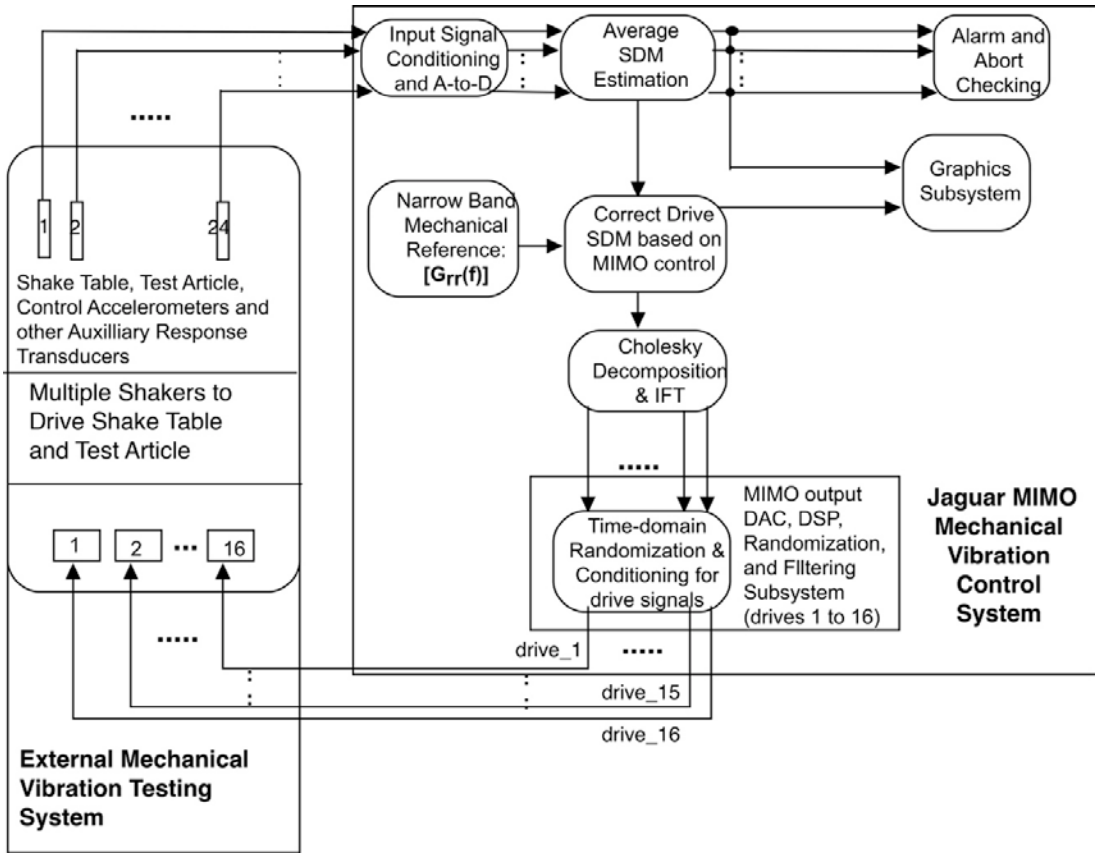

Fig. 2: MIMO Mechanical Vibration Control System

In either mechanical or acoustic MIMO vibration control systems, the degree to which actual test conditions fail to meet the specified test parameters, depends on many factors including the real-world constraints imposed by the system's maximum output capabilities, non-linear response characteristics, time variability in test systems characteristics, limitations on the achievable phase and coherence, limitations of the transducers or exciters employed, as well as constraints imposed by the MIMO vibration test facility and/or associated limitations of the vibration control system.

These limitations collectively contribute to substantial discrepancies between the actual test response and the specified test parameters leading to unreliable test results, damage to the system components or to the test article itself through "over-testing." Prior methods such as described in [7,8,12,13] have mainly focused on establishing limits to prevent the test system from damaging itself or from damaging the test article by minimizing the drive power without regarding the coherence and phase specifications that are present in the pre-specified reference SDM. There have also been ad-hoc methods that change the SDM's off-diagonal terms in manners that affect the quality of the test. In many cases, these minimum drive power and ad-hoc methods often lead to high coherence being specified within the updated reference SDMs synthesized by these methods that are very different from what the test requires [17,22,23,27] and may cause unrealistic test article responses.

In particular, the approaches proposed in [7,8,12,13] attempt to reduce risk of damage to the test system components by using linear system methods to modify the off-diagonal elements of the test's reference Spectral Density Matrix (SDM) to minimize the total drive power, i.e. the trace of the drive SDM or the maximum drive power, to the mechanical or acoustic vibration transducers. These methods attempt to keep the diagonal elements of the specified reference SDM fixed and instead modify the off-diagonal elements of the initial reference SDM to obtain a minimum-drive solution, which often generates off-diagonal elements that yield high-coherence values [7,8,12,13].

Often, the diagonal values of the obtained reference SDM have to be modified in order to keep the resulting reference SDM at least positive semi-definite [20]. This occurs in many cases because these minimum-drive solutions do not necessarily guarantee a positive definite or at least a positive semi-definite modified reference SDM solution [7,8,13]. As a result, these methods require adjustments to the originally specified diagonal values of the specified reference SDM, which may then lead to greater test variance from the desired test conditions. More importantly, these methods do not account for the real-world limitations of the test system and facility, like unavoidable non-linear system behavior, and completely ignore the original specifications for coherence and phase present in the initial control-reference SDM.

Another method discussed in [24] takes steps towards inclusion of real-world parameters in the operation of MIMO vibration control systems for mechanical testing. This method utilizes actual mechanical responses of the test article measured at auxiliary locations other than the control locations to characterize the mechanical transfer functions between the control and auxiliary locations. These field measurements are used to create a new fully populated reference SDM for subsequent testing using the auxiliary locations as control locations instead of the original control locations. This method is very effective in preventing testing using test parameters that may attempt to force the test article to behave in an unrealistic manner, possibly causing significant damage. However, no allowances are made for matching the originally specified reference SDM diagonal elements. The approach also does not account for limitations of the testing system or facility and is not applicable to acoustic testing.

Additionally, [18] introduced rectangular control for MIMO mechanical vibration control systems, without disclosing the underlying optimal adaptive control method. Rectangular Control is also applicable for MIMO acoustic vibration control and was reintroduced [9] by this author in 2009 as part of a modified MIMO mechanical vibration control system for MIMO acoustic testing. However, rectangular control testing, can also fail to account for the real-world limitations of the test system and facility and approximates the initial test specification in the least mean-squared-error sense, sometimes with large discrepancies observed between the pre-specified control-reference SDM and the control-response SDM [18,22], leading to greater test variance from the desired test conditions.

Recently, [27] suggested that it is possible to beneficially incorporate real world constraints imposed by the test system and testing facility, either by using conventional or rectangular control, to achieve improved minimum drive performance and better control performance, although no details regarding how this might be accomplished are disclosed.

Other methods have focused on electronically correcting certain deficiencies in the test system, such as non-linear response. These methods may lead to over-driving. However, as the MIMO vibration control system manipulates drive signals to achieve a match between the test response and the initial test specifications, the additional driving power required for these corrections may exceed system capabilities leading to damage. Such corrective methods combined with system damage limitation schemes also substantially reduce test system capability. In addition, by attempting to correct only certain specific deficiencies in the test system, many other factors are unaddressed or cause new and unforeseen testing problems.

Additionally, there are extended Multiple-Input-Single-Output (MISO) controllers [26], that use multiple conventional MISO controllers independently operating in tandem (some of which within a single control system), with each controller having a MISO controlled output based on the average response of selected subsets of control microphones, all exciting the same acoustic or mechanical system. These systems don't have an ability to control the overall system dynamics, like the dynamic modes that may exist, since they don't have the ability to control the cross-coupling effects that result from exciting a dynamic system with multiple outputs and thus not true MIMO controllers, as discussed in 6.3.3 of [9]. These systems are essentially multiple SISO controllers [9] exciting a single test article that don't have the ability to control the off-diagonal elements of the resulting SDM response and thus can't uniquely control the response of each control channel [9].

The aforementioned issues are common to all fields of vibration testing and specifically DFAT™, RATF, and multi-exciter mechanical vibration testing. Furthermore, the control methods and the underlying control technology are very similar, as can be seen in Figs. 1 and 2. The most notable differences between acoustic and mechanical vibration testing, aside from their field of applicability, is the need to convert n^{th} octave SPL reference spectra and control-response SDMs into and from equivalent narrowband SDMs, while necessarily complying with ANSI S1.11 [26,27] to address the accuracy issues discussed in 6.3.2 of [9], for either DFAT™ or RATF applications, as well as the consideration of

delays and reverberation when controlling an acoustic field response, all of which the method discussed in this paper fully addresses.

Available MIMO (mechanical or acoustic) vibration control systems differ in their basic control methodology, using either the Smallwood [10,11,29] or Underwood [14-16,18,19,29] MIMO control methods. The Smallwood method is based on an adjustable multi-dimensional random noise equalizer [10,11] using conventional control, whereas the complete Underwood method is based on modern optimal adaptive-control [14,15,16] and by extension, minimizes control-error in the LMSE sense while utilizing a minimum power drive SDM [26,27].

Accordingly, it would be advantageous [27] to provide an adaptive MIMO vibration control system with the ability to modify the initial SDM reference specification, for either conventional or rectangular control, according to an empirically determined set of compromises based on the collective limitations of a particular test setup. By using said modified reference SDM specification during actual test operation, an improved match between the test system response and the initial test specification with increased overall capability and reduced risk of damage to the system components or test article would be achieved, regardless of which MIMO vibration control methodology is employed.

Basic Theory Surrounding New Synthesis Method

The new synthesis method creates an optimal reference SDM to be used for MIMO control as shown by Figs. 1 and 2. The method is based on the use of the SDM, which is the generalization of the Power Spectral Density (PSD) to a matrix of the frequency domain functions: the PSD and Cross-Spectral Density (CSD). Just as the PSD, which is a positive (or non-negative) function of frequency that characterizes the power a stationary random process has as a function of frequency, the SDM also characterizes the power a vector of stationary-random processes has as a function of frequency and space, by being a positive-definite or at least positive semi-definite matrix. [17,20,23].

The cross-spectral density matrix (CSDM), on the other hand, is the generalization of the CSD to a matrix of CSDs. Just as the CSD, which is a complex function of frequency, characterizes the joint mutually coherent-power that two stationary random processes have as a function of frequency; the CSDM characterizes the joint coherent-power that two sets of stationary random processes have as a function of frequency [17,20,21,23,25].

The SDM and CSDM contains information that allows us to determine if there exists a linear system connecting any two sets of vectors of stationary random processes and to determine estimates of the frequency response matrix (FRM), [H(f)], that may exist between them [17,20,23]. For example, the following three linear MIMO input/output relationships [20] show how the control-response SDM, $\left[G_{cc}\left(f\right)\right]$, the drive SDM, $\left[G_{dd}\left(f\right)\right]$, and CSDM, $\left[G_{cd}\left(f\right)\right]$, between the control-response, {c(t)}, and its drive, {d(t)}, which are vectors of signals, are connected by a linear MIMO system as follows:

$$\left[G_{cd}(f)\right]=\left[H(f)\right]\left[G_{dd}(f)\right] \quad \text{(Eq. 1)}$$

$$\left[G_{cc}(f)\right]=\left[H(f)\right]\left[G_{dc}(f)\right] \quad \text{(Eq. 2)}$$

$$\left[G_{cc}(f)\right]=\left[H(f)\right]\left[G_{dd}(f)\right]\left[H(f)\right]^{*} \quad \text{(Eq. 3)}$$

Where $[G_{cc}(f)]$, in its off-diagonal CSD terms, contains information on the modal response of the system-under-test and is often used to create Operating Deflection Shape (ODS) displays in experimental modal analysis software [17,20,23]. Higher coherence between control-responses typically requires less drive energy during MIMO control, which is favored by methods described in [7,8,12,13], but at the expense of less control uniformity due to the higher presence of modal response energy in the $[G_{cc}(f)]$ measurement, which can be seen in such ODS displays, and is responsible for the higher coherence.

As for the Single-Input-Single-Output (SISO) case, we can obtain two estimators for [H(f)] from these equations [17,20,23], which are:

$$\left[\hat{H}_1(f)\right]=\left[G_{cd}(f)\right]\left[G_{dd}(f)\right]^{-1}, \text{ the MIMO Type 1 FRM estimator.} \quad \text{(Eq. 4)}$$

$$\left[\hat{H}_2(f)\right]=\left[G_{cc}(f)\right]\left[G_{dc}(f)\right]^{-1}, \text{ the MIMO Type 2 FRM estimator.} \quad \text{(Eq. 5)}$$

It is better to estimate [H(f)] using the Type 1 estimator, since $[G_{dd}(f)]$ is typically known to be invertible and noise free, whereas $[G_{dc}(f)]$ may be singular and $[G_{cc}(f)]$ may be noisy, which often makes the Type 2 estimator less reliable.

The SDM and CSDM matrices also allow us to determine other quantities of interest like the MIMO coherent output power (MCOP) [25], ordinary, partial and total coherence that may exist [18] between two sets of random processes; e.g. the drive vector used to excite a structure and the resultant control-response vector. These will be further discussed and used to analyze the test results from using the new method in subsequent sections.

New Optimal Reference Synthesis Method

The new method is different from previous methods [7,8,12,13], since it uses the underlying multi-dimensional optimization process used for optimal adaptive MIMO closed-loop control, to synthesize the new reference, accounting for any response non-linearity and other such testing limitations that often occur during testing. Previous methods are unable to account for these effects, since they use linear-system response models, based on Eqs. 1-3, for a purely numerical synthesis. Furthermore, the new method only synthesizes Positive Definite Reference SDMs, or at the very least, Positive Semi-Definite SDMs, per the requirements of the test system limitations. The synthesized optimal reference SDMs thus approximates the initially specified reference SDM in the least mean-squared error (LSME) sense, over the test's frequency range, while requiring the least drive power, as functions of the definition of the initially defined reference SDM, while being constrained by the existing testing limitations.

From an initial test conducted with the initially specified reference SDM and the response measurements obtained, the method uses the underlying optimization methodology of the control system to determine how to modify the off-diagonal elements of the pre-specified reference SDM to obtain the newly updated off-diagonal values for the synthesized optimal reference SDM while keeping its diagonal elements unchanged from what was defined within the initial reference, while guaranteeing a P.

Unlike other methods, the new approach accounts for the limitations that may exist in the testing system such as the testing facility; the location of the control transducers and exciters, acoustic or mechanical; and unavoidable non-linear response characteristics that are used as a constraint during the optimization that is used to determine the updated reference SDM to use for subsequent tests. Time variable response characteristics will require the determination of a new optimized reference SDM prior to each such test.

Typically, a more uniform and diffuse acoustic field results in subsequent tests that use the obtained optimal reference SDM for MIMO DFAT™ testing [27]. Reduced control errors for MIMO mechanical vibration testing also result, with more linear test responses and reduced required drive power for both applications, caused by using the more realistic optimal reference SDM, as a consequence of not fighting nature by finding the least-action solution in the Hamiltonian sense for the underlying optimal MIMO control system.

The synthesis of the optimal reference is achieved by using optimal adaptive MIMO closed-loop control to determine what portions of the frequency range of the initial reference SDM's off-diagonal terms need to change as a result of testing limitations. The synthesis method also thus determines how much the off-diagonal terms need to change within these frequency bands to make the newly synthesized reference optimally controllable. The changes are made such that the modified reference remains positive definite or at least semi-definite, but still approximate the initially defined reference SDM in the LSME sense, with the minimum required drive power, as a function of the initially defined reference SDM and the testing limitations that may be present.

A patent filing has been submitted to the U.S. and international Patent Offices for the new optimal reference synthesis method. As such, the method is in a patent pending state. For that reason, further details on the method will be withheld until the patent is granted. However, the description supplied, should help to generally understand how the process works. Later sections present test results from using the new optimal reference synthesis method and analyses using MCOP and partial coherence to demonstrate its benefits.

MCOP Estimation Theory

As presented in [25], MCOP is useful for determining how linear the control-response is, as a result of the MIMO controller drive signals. Thus, MCOP will be used to analyze MIMO system responses in later sections, to better understand the benefits of the new optimal reference synthesis method being discussed. The following discussion of MCOP

and its use of FRM estimation theory will be presented, expanding on what was presented in [25], to better understand its meaning and use.

As presented in [25], for single-input-single-output (SISO) testing coherent output power (COP) theory, the control-response PSD, $g_{cc}(f)$, and the COP PSD, $\hat{g}_{cc}(f)$, are related by:

$$\hat{g}_{cc}(f) = \gamma^2(f) g_{cc}(f) = |g_{cd}(f)|^2 / g_{dd}(f) \quad \text{(Eq. 6a)}$$

where $\gamma^2_{cd}(f) = \dfrac{|g_{cd}(f)|^2}{g_{cc}(f) g_{dd}(f)} = \dfrac{h_1(f)}{h_2(f)}$ is the ratio of type 1 and 2 estimators. (Eq. 6b)

The middle of Eq. 6b is the SISO standard definition of the ordinary coherence between the control-response c(t) and drive-signal d(t) waveforms. In Eqs. 6a and 6b, $g_{cd}(f)$, is the cross-spectral density between c(t) and d(t); $g_{dd}(f)$ is d(t)'s PSD and $g_{cc}(f)$ is c(t)'s PSD; and $h_1(f)$, and $h_2(f)$ are respectively the type 1 and type 2 estimators of the SISO frequency response function between c(t) and d(t) from experimental modal analysis [17,20,23]. Eqs. 6a and 6b imply that the control-response, c(t), can be represented as: $c(t) = \hat{c}(t) + n(t)$, where $\hat{c}(t)$ is the coherent control-response and n(t) is the incoherent response noise-response waveform, typically due to aliasing; mechanical, acoustical or electrical distortion; electrical, mechanical, hydraulic, or numerical noise.

The MIMO coherent output-power (MCOP) SDM, $\left[\hat{G}_{cc}(f)\right]$, can be similarly obtained [25] by generalizing Eq.6a, but with particular attention to the matrix operation order, as:

$$\left[\hat{G}_{cc}(f)\right] = \left[G_{cd}(f)\right]\left[G_{dd}(f)\right]^{-1}\left[G_{cd}(f)\right]^{*} \quad \text{(Eq. 7a)}$$

Where the MCOP SDM $\left[\hat{G}_{cc}(f)\right]$ plays a similar role as the SISO COP PSD, $\hat{g}_{cc}(f)$, but generalized for MIMO testing [25]. However, [25] does not present many of the details on how Eq. 7 is obtained. It can be derived for the MIMO case, if we combine the expression for the $\left[\hat{H}_1(f)\right]$ FRM estimator from Eq. 4, with Eq. 3, to obtain:

$$\begin{aligned}\left[\hat{G}_{cc}(f)\right] &= \left[\hat{H}_1(f)\right]\left[G_{dd}(f)\right]\left[\hat{H}_1(f)\right]^{*} \\ &= \left[G_{cd}(f)\right]\left[G_{dd}(f)\right]^{-1}\left[G_{dd}(f)\right]\left[G_{dd}(f)\right]^{-1}\left[G_{cd}(f)\right]^{*} = \left[G_{cd}(f)\right]\left[G_{dd}(f)\right]^{-1}\left[G_{cd}(f)\right]^{*}\end{aligned} \quad \text{(Eq. 7b}$$

Thus obtaining Eq. 7a in the lower right-hand side of Eq. 7b. As for SISO systems, the control-response vector, {c(t)}, for MIMO systems can also be represented by: $\{c(t)\} = \{\hat{c}(t)\} + \{n(t)\}$, where $\{\hat{c}(t)\}$ is the coherent component of the control-response vector, $\{c(t)\}$, and $\{n(t)\}$ is a vector of uncorrelated noise waveforms, i.e. its non-coherent response. $\{n(t)\}$ is also typically due to aliasing; acoustic, mechanical and/or electrical distortion; electrical, mechanical, hydraulic and/or numerical noise; and/or any

other nonlinear effect. The coherent control-response vector, $\{\hat{c}(t)\}$, thus represents the linear response due to the MIMO drive vector's, $\{d(t)\}$, excitation.

Since $\{\hat{c}(t)\}$ and {n(t)} are uncorrelated by design, we can also similarly represent $[G_{cc}(f)]$ as: $[G_{cc}(f)]=[\hat{G}_{cc}(f)]+[G_{nn}(f)]$, which decomposes $[G_{cc}(f)]$ as the sum of the coherent response SDM, $[\hat{G}_{cc}(f)]$, and the SDM of the incoherent noise response vector, $[G_{nn}(f)]$, similar to what was discussed in conjunction with Eqs. 6a and 6b.

We can also obtain expressions for what could be called MIMO ordinary coherence, $[\Gamma_{cd}(f)]$, where one of these expressions is based on the coherent control-response SDM, by generalizing the basic definition of coherence as the following function of the matrix type 1 and type 2 estimators, which is similar to the ratio of estimators in Eq. 6b, as:

$$[\Gamma_{cd}(f)]=[\hat{H}_1(f)][\hat{H}_2(f)]^{-1} = [G_{cd}(f)][G_{dd}(f)]^{-1}[G_{cd}(f)]^{*}[G_{cc}(f)]^{-1}=[\hat{G}_{cc}(f)][G_{cc}(f)]^{-1}=[I]-[G_{nn}(f)][G_{cc}(f)]^{-1} \quad \text{(Eq. 8)}$$

Where $[I]$ is the identity matrix and the last term behaves like a noise-to-signal ratio. Using the middle part of Eq. 8 provides an alternate formulation, which yields an expression for $[\hat{G}_{cc}(f)]$, which is similar to Eq. 6a for SISO, and which is given by:

$$[\hat{G}_{cc}(f)]=[\Gamma_{cd}(f)][G_{cc}(f)] \quad \text{(Eq. 9)}$$

A dual expression for MIMO ordinary coherence can also be obtained from the previous research, but which will not be discussed in detail, since it's not central to MCOP theory. It instead is related to a dual-problem, e.g. determining a coherent drive $[\hat{G}_{dd}(f)]$ that is linearly related to $[G_{cc}(f)]$.

It is given by:

$$[\hat{\Gamma}_{dc}(f)]=[\hat{H}_2(f)]^{-1}[\hat{H}_1(f)] =[G_{dc}(f)][G_{cc}(f)]^{-1}[G_{dc}(f)]^{*}[G_{dd}(f)]^{-1}=[\hat{G}_{dd}(f)][G_{dd}(f)]^{-1} \quad \text{(Eq. 10a)}$$

Note that the order of the subscripts "c" and "d," the order of the type 1 and type 2 estimator operations, and the complex conjugate-transpose operations have been switched in Eq. 10a to motivate the following coherent drive input SDM discussion. The coherent drive input SDM, $[\hat{G}_{dd}(f)]$, is similar to coherent control-response that is obtained by:

$$\left[\hat{G}_{dd}(f)\right]=\left[G_{dc}(f)\right]\left[G_{cc}(f)\right]^{-1}\left[G_{dc}(f)\right]^{*}=\left[\hat{\Gamma}_{dc}(f)\right]\left[G_{dd}(f)\right] \quad \text{(Eq. 10b)}$$

Partial Coherence

For MIMO control systems, there is a need to determine the partial coherence between each of the drive signals used to control the response of a MIMO test and any one of the control-responses associated with those drives [21], to see how linear the responses are. For example, one may wish to determine the partial coherence of the jth drive and the ith control, where there are N drives and M controls. In that case, as [21] discusses, one forms an SDM, $[G_{xx}(f)]$, from the elements of the SDMs $[G_{cc}(f)]$ and $[G_{dd}(f)$; and the CSDM $[G_{cd}(f)]$, as follows:

$$\left[G_{xx}(f)\right]=\begin{bmatrix} g_{c_ic_i}(f) & \begin{bmatrix} g_{c_id_1}(f) & g_{c_id_2}(f) & \cdots & g_{c_id_N}(f) \end{bmatrix} \\ \begin{bmatrix} g_{d_1c_i}(f) \\ g_{d_2c_i}(f) \\ \vdots \\ g_{d_Nc_i}(f) \end{bmatrix} & \left[G_{dd}(f)\right] \end{bmatrix} \quad \text{(Eq. 11)}$$

Using this form of the SDM $[G_{xx}(f)]$, one can then compute the partial coherence between the ith control and the jth drive, $\gamma^2_{c_i,d_j\cdot d_1,\ldots,d_{j-1},d_{j+1},\ldots,d_N}(f)$, with the linear effects of the remaining drives, $\left\{d_1(t),\ d_2(t),\ \ldots,\ d_{j-1}(t),\ d_{j+1}(t),\ \ldots,\ d_N(t)\right\}$, removed. One can use the following Eq. 12 for its determination, where [21] has the details of the minors $M_{1,j+1}(.)$ and $M_{j+1,j+1}(.)$ that are used.

$$\gamma^2_{c_i,d_j\cdot d_1,\ldots,d_{j-1},d_{j+1},\ldots,d_N}(f)=\frac{\left|M_{1,j+1}\left(\left[G_{xx}(f)\right]\right)\right|^2}{\det\left(\left[G_{dd}(f)\right]\right)M_{j+1,j+1}\left(\left[G_{xx}(f)\right]\right)} \quad \text{(Eq. 12)}$$

Note that because of the special way in which $[G_{xx}(f)]$ is formed, we use the minors $M_{1,1}([G_{xx}(f)])$, which is equal to $\det([G_{dd}(f)])$, and $M_{1,j+1}([G_{xx}(f)])$ in the previous equation. In Eq. 12, as [21] explains, we use the index "1" because we are placing the contribution of the ith control signal into the first row and column of $[G_{xx}(f)]$ and also use the index "j+1," since we place the contribution of the jth drive into the (j+1)th row and column of $[G_{xx}(f)]$, as shown in Eq. 11, instead of the general, but more cumbersome formulation that is described in [21]. Eq. 12, on the other hand, is optimized to determine the partial coherence between individual drives and individual control-response signals for MIMO control systems, which is used to obtain the partial-coherence results. To compute the partial coherence of another control, say the kth control, with respect to the jth drive, we substitute $g_{c_kc_k}(f)$ for $g_{c_ic_i}(f)$ and also $g_{d_nc_k}(f)$ for $g_{d_nc_i}(f)$, for n=1 to N, in Eq. 11 and again use Eq. 12 for its determination.

The above process, when taken to its full generality, will yield a full matrix of partial coherences, $\gamma^2_{c_i,d_j \cdot d_1,\ldots,d_{j-1},d_{j+1},\ldots,d_N}(f)$, where i=1 to M and j=1 to N, in the case where we have M control signals and N drive signals, as in rectangular control as discussed in [18,21,22]. Each element in this partial coherence matrix, $\gamma^2_{c_i,d_j \cdot d_1,\ldots,d_{j-1},d_{j+1},\ldots,d_N}(f)$, represents the partial coherence between the ith control and jth drive, by removing the **linear** effects of all the other drives on the ith control with the above set of operations in Eq. 12. Like with ordinary coherence, high values close to 1 for partial coherence indicates a high linear relationship between the jth drive sand the ith control signal [21].

Note that since we are dividing by the determinant of the drive's SDM, $[G_{dd}(f)]$, in Eq. 12, the calculation will become ill-conditioned at frequencies where the coherence between drives approaches one, reflecting the fact that the drives become essentially indistinguishable [20,21]. When measuring the partial coherence between the drives and particular control-responses, it's a good idea to not use fully coherent drives.

It has been found by testing that coherence between drives as high as 0.95 will still result in a well-conditioned calculation [21], so long as the determinant calculation has been optimized, as the implementation used to obtain the to be discussed partial-coherence results demonstrates, which use a matrix decomposition approach to optimize the determinant and minor calculations.

Additionally, care in the calculation of the respective matrix minors that are used in Eq. 12 is necessary to yield credible results, when the various matrices that are used in the calculation become singular or nearly singular. Use of nearly singular matrices should thus be avoided. Ref. [21] has other examples where the determination of partial coherence will also depend on the relative phase between drive signals.

Previous MIMO DFAT™ Test Results

These test results are discussed to provide a baseline for the improvements that using the new optimized reference SDM provide. These previous results were obtained using narrow-band, Fast Fourier Transform (FFT) based digital filtering, and modern adaptive optimal MIMO control [26]. The tests were performed from 20 Hz to 10kHz using Δf=3.125Hz, using digitally synthesized ANSI S1.11 standard 1/3rd octave band pass-filters [26,27]. The previous test results were obtained using 15 Independent Drives, digital mixers and 15 control microphones. More drives and controls have been used on other such tests in the past.

We've (SD, MSI DFAT, and this author) [9] have conducted many public tests demonstrating the testing capability and testing results that will be presented. Refs. [4,6,26,27] contain additional test results that show the ability to control the magnitude of standing waves, as discussed in [3,9], using the advanced adaptive optimal control of the MIMO acoustic control system that has been developed. We also use, in addition to the control microphones, additional monitor and array microphones, to verify the achieved acoustic field uniformity [9], at non-control locations throughout the achieved acoustic

field. Advanced optimal adaptive control and randomized microphone placement are used to reduce the magnitude of standing acoustic waves to reduce structural "Hot Spots" [3,9] and help provide the resulting acoustic field uniformity.

The following Fig. 3 shows the PSDs of 15 control and 21 monitor microphones resulting from a previous MIMO DFAT™ test overlaid, in pa^2/Hz units, which show excellent uniformity. The uniformity of the 36 microphone PSD responses demonstrates the control of the acoustic modes in the resulting acoustic field that the advanced adaptive MIMO control and specialized sound system designs by MSI DFAT has made possible.

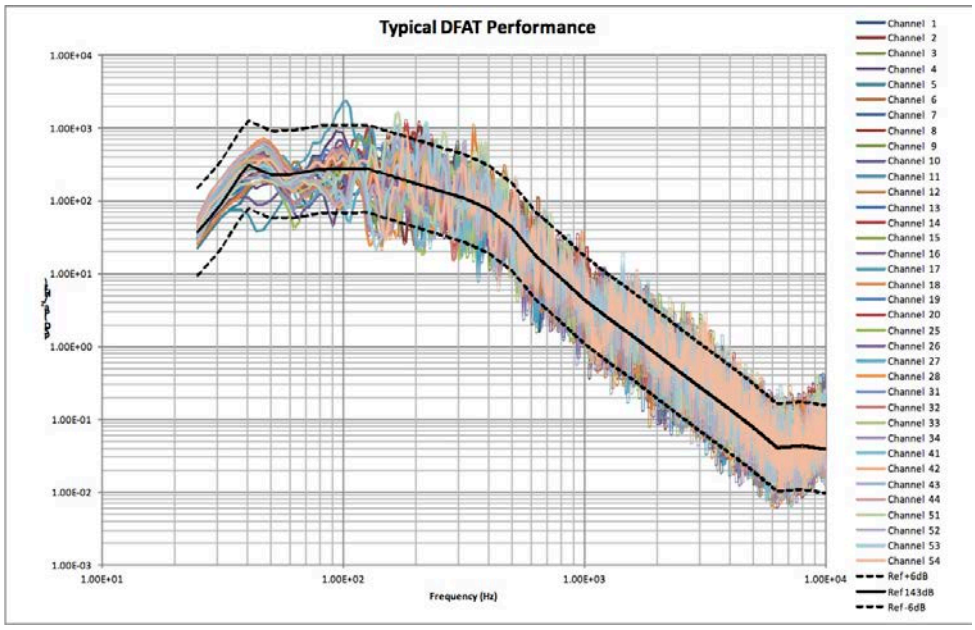

Fig. 3: Previous Results with 15 Speaker Stacks & 15 Control Mic.'s

New Optimal Reference Synthesis Method Testing Result Discussion

The following testing results are from the use of the previously described new control-reference SDM synthesis method, developed and implemented within the Jaguar MIMO acoustic control system shown in Fig. 1, using the same speaker stack and control-microphone configuration as were used for the Fig. 3 results. As described previously, the new method yields a modified optimal reference SDM, which approximates the specified control-reference SDM in the LSME sense requiring the least drive power, as a function of the pre-specified control-reference SDM, which specifies a fully diffuse (low-coherence) acoustic field [9], while addressing testing system and facility limitations.

The use of the optimal control-reference SDM for a subsequent acoustic test causes the control system to produce a drive SDM that requires the least drive power to achieve the least approximation error to the pre-specified diffuse acoustic field control-reference SDM. That optimal control-reference SDM is due to the use of advanced adaptive optimal-control methods by the MIMO DFAT™ control-system, which is a function of the definition of the pre-specified control-reference SDM and of the previously discussed limitations in the testing system.

The result of this optimal control, in conjunction with the use of the new optimized SDM, is that it provides a more uniform and diffuse acoustic field for DFAT™ than what we were previously able to obtain. The net result is better control of both the acoustic levels in terms of PSD and 1/3rd octave SPL spectra, as well as of the response coherence and phase between control microphones relative to the newly optimized control-reference SDM.

The multi-dimensional control optimization that the MIMO DFAT™ control system employs, is performed each control loop iteration using the control system's inherent optimal adaptive MIMO control optimization methodology. It's not simply an n-dimensional noise equalizer as other MIMO control systems employ.

A further benefit of using the newly developed optimized control-reference SDM synthesis method is that it results in a more linear response characteristic, due to the reduced power demands as well as the use of a more realistic control-reference SDM that the new synthesis method provides, which will be more fully discussed in a later section.

Results using Optimized Reference for Acoustic Testing

Figs. 4 through 6 illustrate these recent improvements in controlling 15 speaker stacks using rectangular control [18,20,22] with four drives and 15 control microphones, with the same configurations as what were used for the testing results discussed for Fig. 3. The two-integer bracketed indexes following the identification of the plotted spectral-traces, are SDM spectral element indexes, which refer to matrix elements corresponding to microphone pairs. Fig. 4 shows the average of all 15 control-microphones in both PSD and SPL acoustic spectrum formats in black, demonstrating how well the average of control-microphone responses agree with their respective reference spectra in green. Fig. 4 also shows that the response PSD spectra are smooth within their respective nth octave band, which is not true for conventional nth octave band control [26,27].

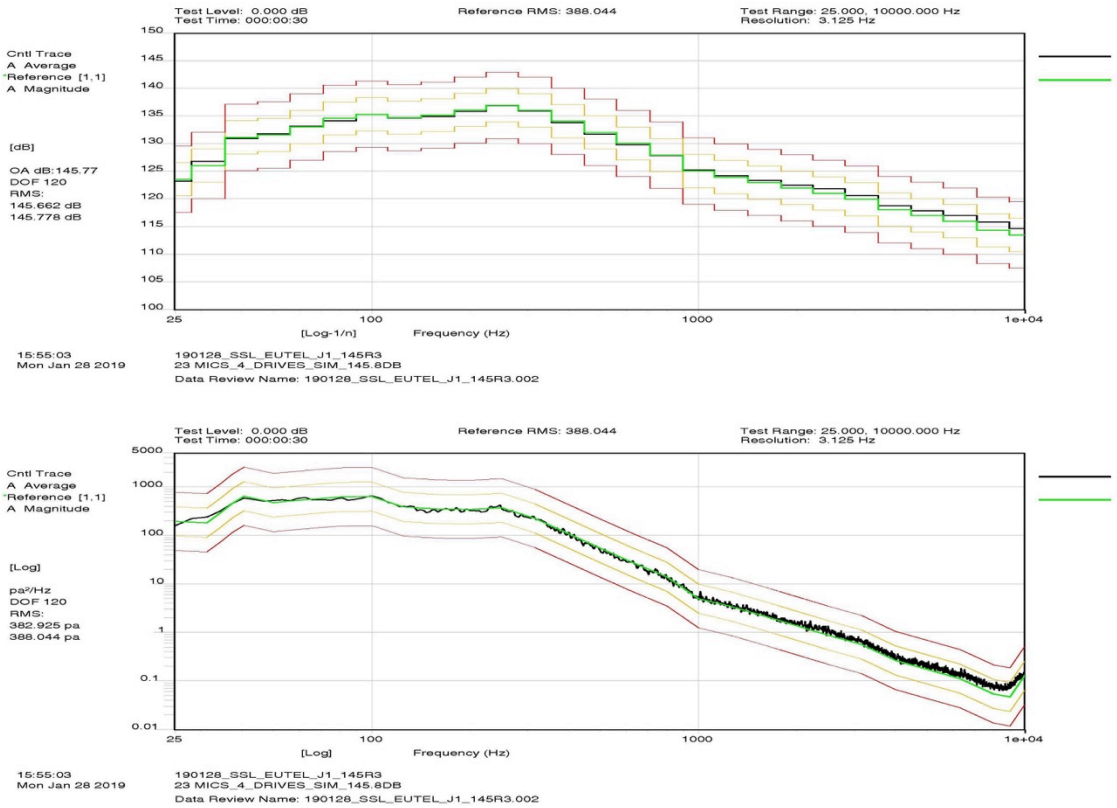

Fig 4: Average of 15 Controls – SPL & PSD, using optimized control-reference SDM

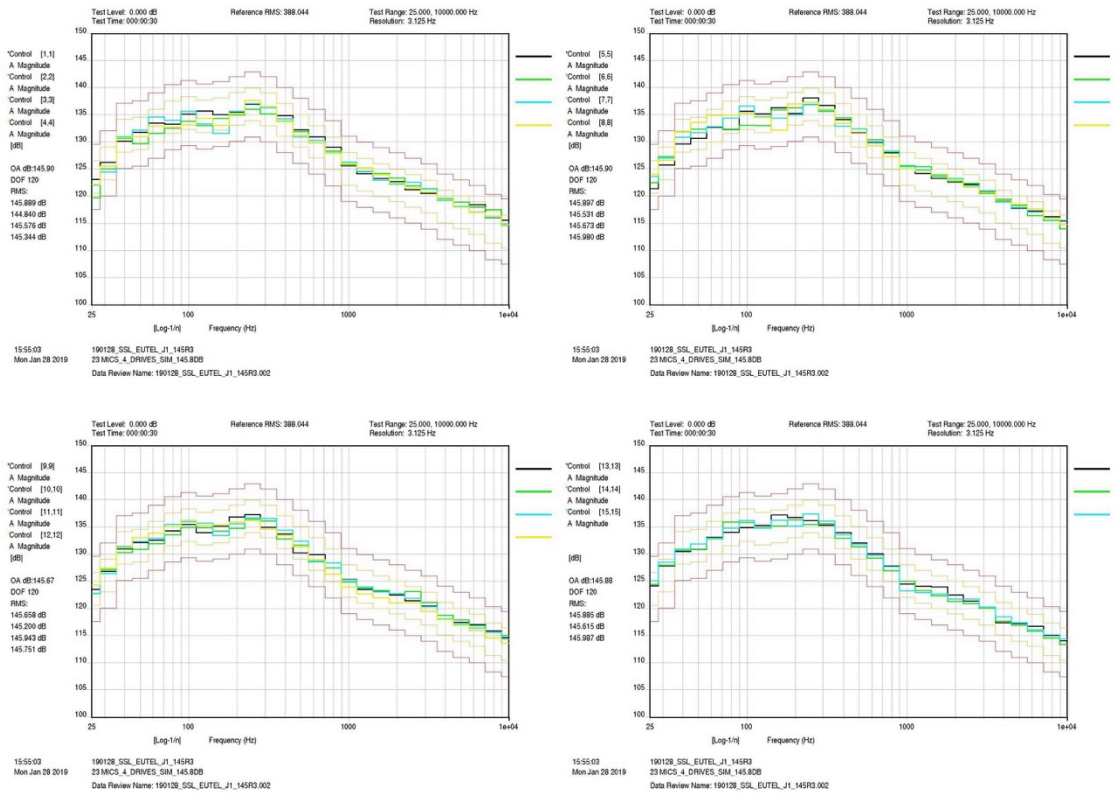

Fig 5: Control Microphones - 1 through 15 – 1/3rd Octave Acoustic Spectra

The previous Fig. 5 demonstrates how well the individual SPL acoustic spectra of the 15 control-microphones match each other and their respective control-reference, showing the significant improvements in the uniformity of the resulting acoustic field. The following Fig. 6 shows nearly zero relative coherence achieved between typical control microphones, except as limited by microphone spacing, demonstrating nearly diffuse acoustic field responses. Note the higher coherence values at the lowest frequencies for closely spaced microphones, which approximate the sinc^2 function shape as expected for nearby microphones (a characteristic of diffuse acoustic fields [2]), like between 1 and 2; 3 and 4; 1 and 9; and 1 and 10, but much lower between microphones that are separated by greater distances, which is due to the longer wavelengths at the lower frequencies, which similarly affect nearby microphones leading to their higher relative coherence at low frequencies [28]. The optimized SDM reference contains considerations for that effect in the determination of its off-diagonal elements, which properly accounts for the distance between control microphones [28]. When used as the control-reference SDM it helps the control system provide an LMSE approximation to what is expected from the achieved coherence between control microphone response, as shown by the following Fig. 6.

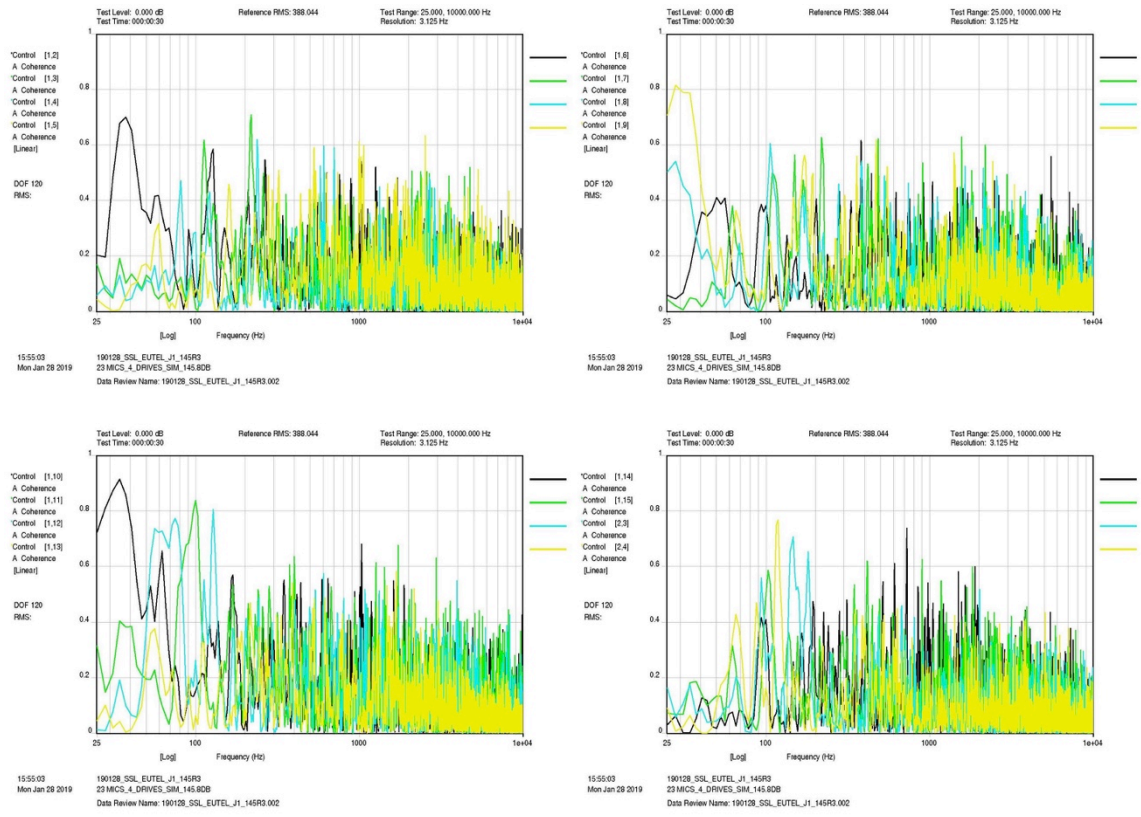

Fig 6: Coherence Results – Microphone 1 vs. Microphone 2 to 15

These improvements in control performance shown by Fig. 4 through 6 are mainly the result of the discussed adaptive optimal control and the use of new optimization process that is used to set the coherence and phase off-diagonal elements in the new synthesized control-reference SDM to approximate what is expected from a diffuse acoustic field [2,9], by properly accounting for the placement and distances between microphones and speakers;

the acoustic modes present within the test area; as well as other limitations that may be present in the acoustic testing facility and its associated equipment.

Further Improvements in DFAT™ Performance by New Optimal Control Methods

These improvements in performance, as shown by the previously described results, are largely due to the discussed adaptive optimal control and the new optimization process used to set the coherence and phase off-diagonal elements in the new synthesized optimal control-reference SDM. As has been stated, the optimized reference that the new method produces, accounts for the location of the microphones and speakers; the distances between microphones and speakers; the acoustic modes present within the test acoustic field; as well as other limitations that may be present in the acoustic testing facility and its associated equipment, as demonstrated by the better result that were obtained with its use.

Optimal Adaptive Control Results in Least Mean Squared Error and Drive Power

The discussed optimal adaptive control and optimized reference SDM enables the MIMO acoustic control system, employing the new optimized reference, to further reduce the control error as well as the power needed to drive the multiple speaker stacks. The following Figs. 7a, 7b, and 7c demonstrate that we have achieved the same test level and coherence with fewer speaker stacks from using the new optimized control methods and further improvements made to the loudspeaker technology that is used by MSI DFAT.

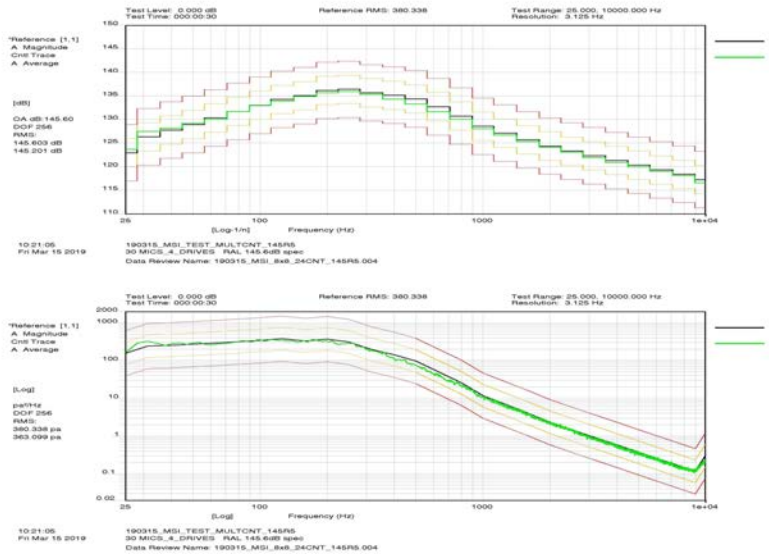

Fig. 7a: Avg. 1/3rd Octave SPL & PSD Using 8 Speaker Stacks & 24 Control Mic's

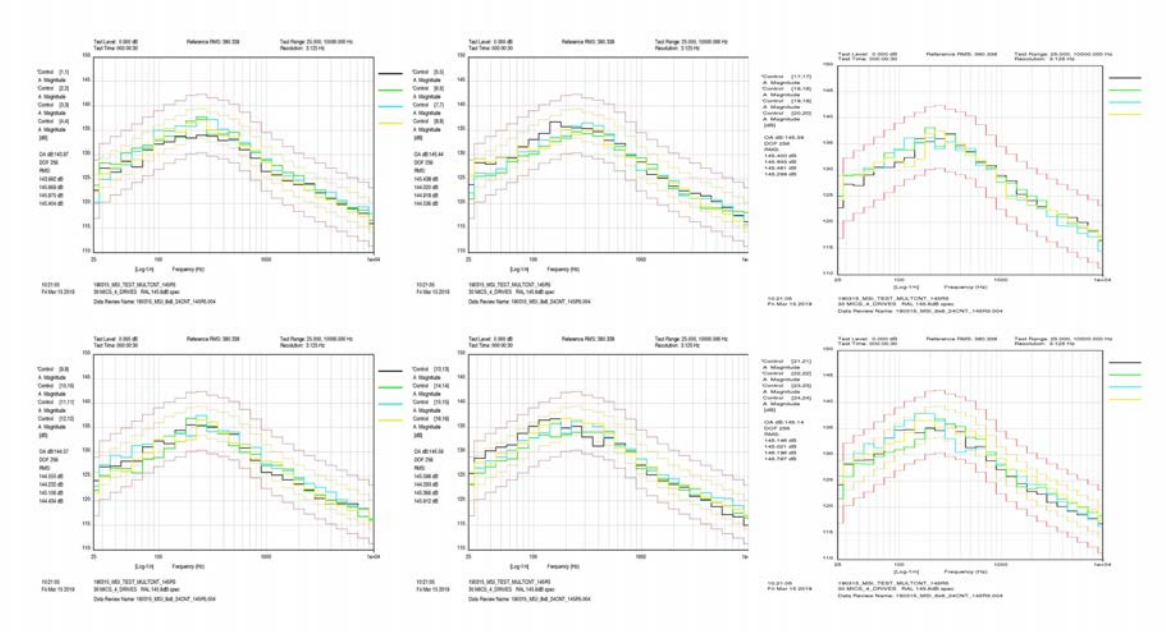

Fig. 7b: 24 Controls using 8 Speaker Stacks & 24 Control Microphones

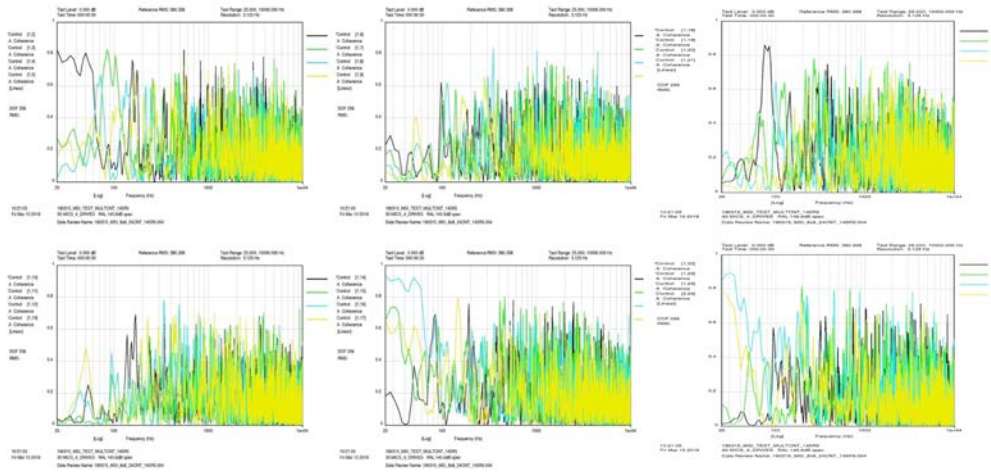

Fig. 7c: Coherence Results Using 8 Speaker Stacks & 24 Control Microphones

The improvement in acoustic field uniformity, as well as the better approximation to a diffuse acoustic field response, shown by Figs. 4, through 7c, support these claims, since the improvements are a result of the adaptive optimal control, as demonstrated by the discussions about Fig. 7d in the next section, which inherently provide the least drive power SDM, to attain the least mean-squared control error for a given acoustic power requirement and initial reference SDM definition.

Overall, these results also show that the acoustic field response is further optimized using the discussed minimum drive-power reference SDM and enhanced loudspeaker technology, particularly comparing Figs. 7a through 7c with Figs. 4 through 6, since the results in Figs. 4 through 6 use 15 speaker stacks using the previous loudspeaker

technology and 15 control-microphones, whereas the results in Figs. 7a through 7c uses 8 newer technology speaker stacks and 24 control-microphones, while achieving the same acoustic OA SPL. The results shown by Figs. 4 through 7c, show a nearly uniform diffuse acoustic-field with the least mean-squared control error and the least drive power.

Further Reductions in Required Drive Power

Since the optimized reference synthesis depends on the initial reference definition that is used in a non-linear manner, it has been verified that by slightly increasing the initial values for the coherence spectra from zero to a small positive value in the lowest frequencies, can create significant power savings, at the expense of slightly lower uniformity and diffusivity in the resulting control-responses, where this decrease follows the increase of the initial reference coherence in a non-linear fashion. Thus, it is possible to trade-off these two values, i.e. further reduce the power needed to reach a prescribed SPL against how well the response sound pressure levels approximates a uniform diffuse acoustic field. It was confirmed that slight increases of coherence decreased the uniformity of control-microphone responses on the order of no more than 0.5 dB. The following Fig. 7d shows the decrease of the drive power of the 4 drives after a slight increase in the initial reference spectrum definition's relative coherence between 20 Hz and 50 Hz.

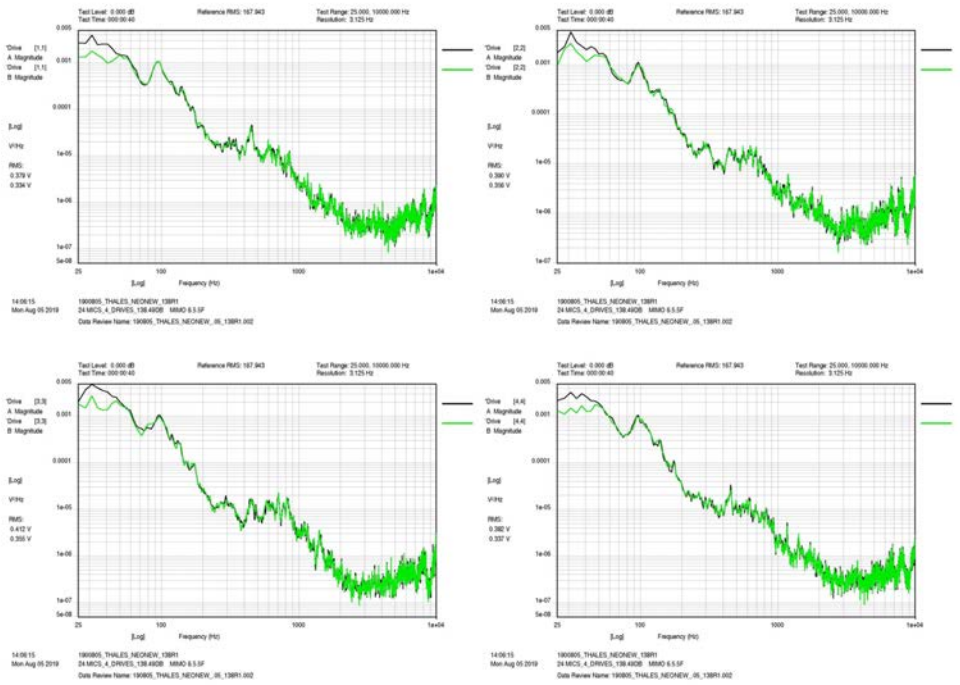

Fig. 7d: Reduction of Drive Power as a Result of Increasing Coherence Slightly

The black traces for the PSDs for Drives 1 through 4, represent the drive power, as a function of frequency, needed to reach the full-test level, when the initial reference coherence between all of the 24 control microphones that were used for this research test were defined to zero, i.e. to achieve a perfectly diffuse acoustic field response, and the corresponding green traces are for a similarly defined test, but where the initial reference

coherence between control microphones was increased slightly above zero between 20 Hz and 50 Hz. Note that the sound system's drive PSDs for the green traces are lower than the corresponding black traces, by as much as a factor of 3 for drives 1, 3, and 4 between 20 Hz and 50 Hz. The corresponding spread in the control responses, although not shown, increased no more than 0.5 dB, indicating a good tradeoff between drive reduction and control response uniformity and diffusivity was attained, where the response coherence between control microphones increased by no more than 5% for this test and facility. This improvement will depend on the limitations that may exist in individual facilities due to the non-linear dependence between such changes in the coherence and the test response that is obtained. However, these changes to the initial reference coherence can provide a higher response sound pressure level for the same drive power, if not otherwise possible.

Importance of achieving a near Diffuse Acoustic Field to use for Testing

As in known by many in acoustic testing, a structure tested with a nearly diffuse (incoherent) acoustic field, responds as if the structure is being excited by a distributed force field, with a very large number of uncorrelated exciters having random angles of incidence. RATF provides that capability, but at a significant cost [1], but also with DFAT™ using the discussed optimal adaptive control technology demonstrated Figs. 7a through 7c. On the other hand, a structure tested with a non-diffuse (highly coherent) acoustic field, responds as if the structure is being excited by a distributed force field, with numerous correlated exciters, with nearly fixed angles of incidence. It should be clear from these discussions that a diffuse acoustic field is better at exciting all of the externally excitable resonances of a given structure than a non-diffuse acoustic field, which provide a better qualification acoustic tests for significant structures like Satellites and their components that's consistent with previous RATF results. Recent testing results demonstrated this fact.

As an example of the structural response differences between testing with a near diffuse acoustic field and non-diffuse acoustic fields, Fig. 7e, as explained by [28], shows the PSD response for A3, one of the 10 accelerometers mounted on an aluminum honeycombed 4'x8' panel plate, that was tested with 4 different acoustic field excitations from: 1) Test R5A, like the acoustic test described by Figs. 7a through 7c, but with an OASPL of 138.5 dB, and 3 tests creating non-diffuse acoustic fields: 2) Test R5B non-diffuse (high coherence between all 24 control microphones), 3) Test R4A Directional Coherent Field (high coherence between all 24 control microphones and phase settings to create a directional coherent field excitation normal to the plate superimposed on a diffuse field), and 4) Test R5E MISO control generated acoustic fields (coherence and phase spectra off-diagonal element response not controlled, whose values are dependent on the acoustic modal structure of the room, speaker and microphone configuration, and test article interaction), with all 4 tests using the same reference 1/3rd octave SPL spectra at 138.5 dB OASPL, but the last 3 tests using higher coherence settings for the off-diagonal elements of their respective initial control-reference SDM as described. Consult [28] for testing details and the complete analysis of the PSD responses for all 10 panel mounted accelerometers.

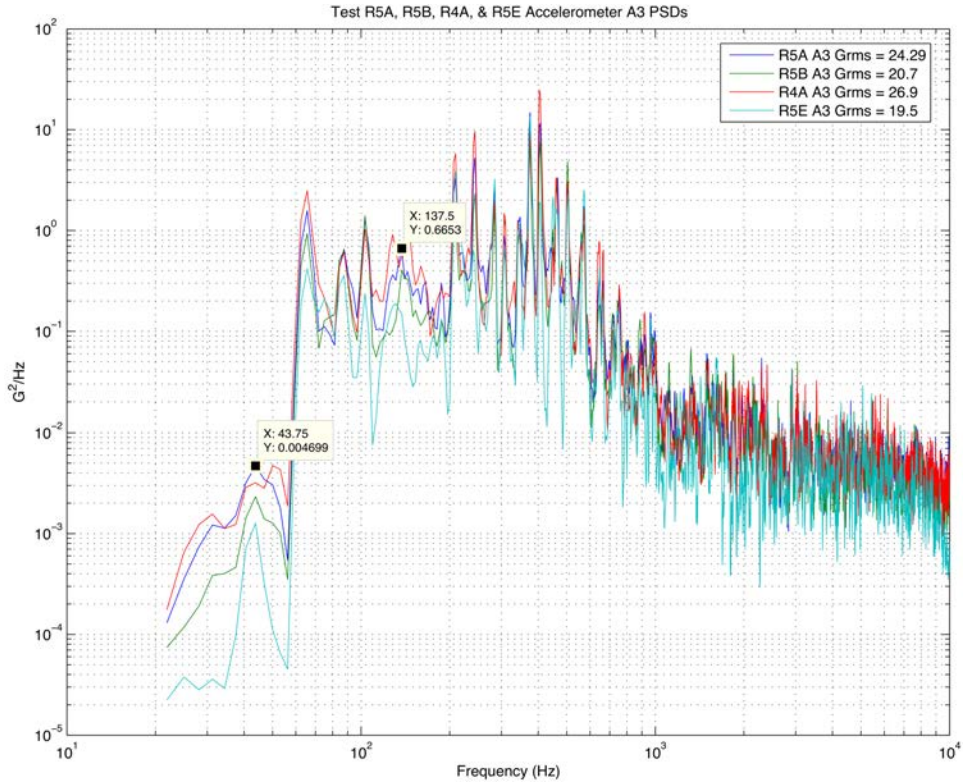

Fig. 7e: A3 PSD Comparison for Tests R5A, R5B, R4A, and R5E

After the 4 acoustic tests concluded, a Modal Test and subsequent Modal Analysis was performed on the panel plate test structure to determine its first 16 modes, natural frequencies, damping, and the corresponding damped resonance frequencies. The accelerometer response PSDs recorded during the 4 acoustic tests showed that Test R5A did the best job of exciting and identifying resonances close to the damped resonance frequencies predicted by the Modal Analysis [28]. A good example of this is demonstrated by the response of the resonances at 43.8 Hz and 137.5 Hz shown in Fig. 7e for the PSDs obtained from A3 during Tests R5A, R5B, R4A, and Test R5E.

Note that only Test R5A excites the resonance at 43.8 Hz properly and that Test R4A causes a dip at that frequency and a resonance peak at just under 60 Hz, i.e. a "phantom" resonance. At 137.5 Hz the discrepancies are greater, where Test R5B creates a double peak just past 137.8 Hz, around 143.8 Hz, and Test R4A creates "phantom" resonances before and after 137.5 Hz, i.e. at 128.1 Hz and 143.8 Hz, with a strong dip at 137.5 Hz, i.e. examples of response enhancement and cancellation.

MISO Test R5E is by far the worst performer in general, as seen in Fig. 7e. Test R5E exhibits the lowest resonant response at 43.8 Hz, the lowest frequency resonance identified by Modal Analysis, and no resonant response caused at 137.5 Hz, but instead a "phantom" resonance at 128.1 Hz. Fig. 7e also shows that Test R5E caused the lowest resonance response for all identified 16 resonances, as compared to the other three tests in general, with many resonances not showing at all [28].

Fig. 7e illustrates the fact that all three non-diffuse acoustic field excitations of the tested structure exhibit both response cancellation and enhancement effects at many resonances, which is a general characteristic of non-diffuse acoustic field excitation, as demonstrated by the A3 PSD response results displayed by Fig. 7e [28].

Summary of Findings

- The new synthesized optimal control-reference SDM matches the initially specified reference in the LMSE sense, subject to its definition and testing system limitations.
- The use of the new synthesized control-reference SDM also reduces the dependence of microphone and speaker placement on standing wave control performance.
- As a result, new DFAT™ results have improved uniformity via rectangular control by using this minimum drive power reference SDM, while approximating a diffuse acoustic field in the LMSE sense.
- Improved uniformity and lower achieved relative coherence and better phase matching between microphones, as compared to previous DFAT™ results.
- Results show better uniformity of control and monitor microphone responses as well as a better approximation to a uniform diffuse acoustic field than previous methods.
- Acoustically induced vibration test results show that the achieved diffuse acoustic field better excites structural resonances than non-diffuse acoustic fields.
- The new minimum drive-power reference SDM is obtained by the control system's inherent optimization methods used by its adaptive optimal control and new research.
- Better rectangular control uniformity and lower achieved coherence between control-microphones over the control frequency range.
- New testing results show that the new minimum drive-power reference SDM synthesis method further improves on rectangular control, by accounting for limitations in the test system and facility.

Multi-DOF Shaker Control Vibration Test Results Using Optimized Reference

In the following, we ran two tests to compare the results from Multi-Shaker testing using the newly developed optimized reference to testing results without the benefit of the new optimized reference. To compare these tests, we configured a difficult testing system comprised of 5 Shakers with 5 rigid-body degrees-of-freedom (DOFs): 1-X, 2-Y, 2-Z, 2-R_z, and 2-R_y, i.e. 3-orthogonal translation axes and 2-orthogonal rotational axes [19].

The following Fig. 8, has a photo of the 5-shaker system and simulated device-under-test (DUT). As Fig. 8 shows, stingers are used to decouple the 5 shakers from each other, serving as the interface between the shakers and DUT via the shown brackets. In this way the stingers and shakers can create the 5-independent rigid-body DOFs of motion, X, Y, Z, yaw (R_z), and pitch (R_y) [19]. The decoupling is accomplished by using the fact that stinger bending stiffness is much lower than their axial stiffness, allowing each shaker to move along their line of force without significantly affecting the other shakers, while still efficiently applying their individual forcing function to the DUT along its designated axis.

However, the stingers and bracket attachments are not ideal and exhibit non-linear responses accompanied with rattling and loosening of the couplings during the test as well as their associated modal response characteristics, which act as additional independent noise generators. As a result, control of PSD and coherence is difficult and low partial coherence between drives and controls occurs at many frequencies by design.

Also by design, the reaction masses were inadequate, as the shakers simply rested on plates on the floor or boxes, held in place by their static friction. The test article (DUT) consisted of a PVC plumbing pipe section attached to the end of the stingers as shown in Fig. 8. The alignment of the shakers was also not precise to make the testing results have more non-linear effects, along with the other problematic effects that have been described.

Fig. 8: Multi-Exciter Test Article

The shakers were driven by audio class power amplifiers, with adequate power to drive the chosen shakers. Fig. 8 shows the resulting overall testing system. These testing system problems were used to test the effectiveness of the new method with real-world problems.

MIMO Random Tests

The two tests were run, identically defined with different shaped PSD profiles for each axis, and all profiles set to 1 Grms to conduct a three-axis (X, Y, and Z) test, with all three

axes uncorrelated with each other and suppressing the two rotations R_z and R_y [19]. The initial pre-specified reference SDM was defined with coherence set to 0.9 and zero phase between similar axes to suppress rotations [19], for the two shakers driving each of the Y and Z axis, and zero coherence between the independent Y, Z, and the single shaker X axes for uncorrelated motion between the X, Y, and Z axes [22].

The two tests were run for 15 minutes each, with aborts disabled to better detect any problems with testing that might occur, as couplings loosen during the testing. Test A used the original pre-specified control-reference SDM and Test B used the optimized control-reference SDM obtained with the new method. The couplings were re-tightened between tests so that each test started with the same pre-test structural conditions.

An initial low-level test was run prior to Test B to determine the new optimal synthesized control-reference SDM from this test using the pre-specified reference SDM as previously described. Once this low-level test was run and the optimal control-reference was determined, it was loaded into the system to be used as Test B's control-reference SDM. The following Fig. 9, shows the comparison of Test A's and B's Y-axis and Z-axis test results for PSD and coherence response, each driven with two shakers and using the same two sets of two accelerometers, at the end of each 15-minute test. Relative phase is not presented since relative coherence is the most sensitive to the cited testing problems.

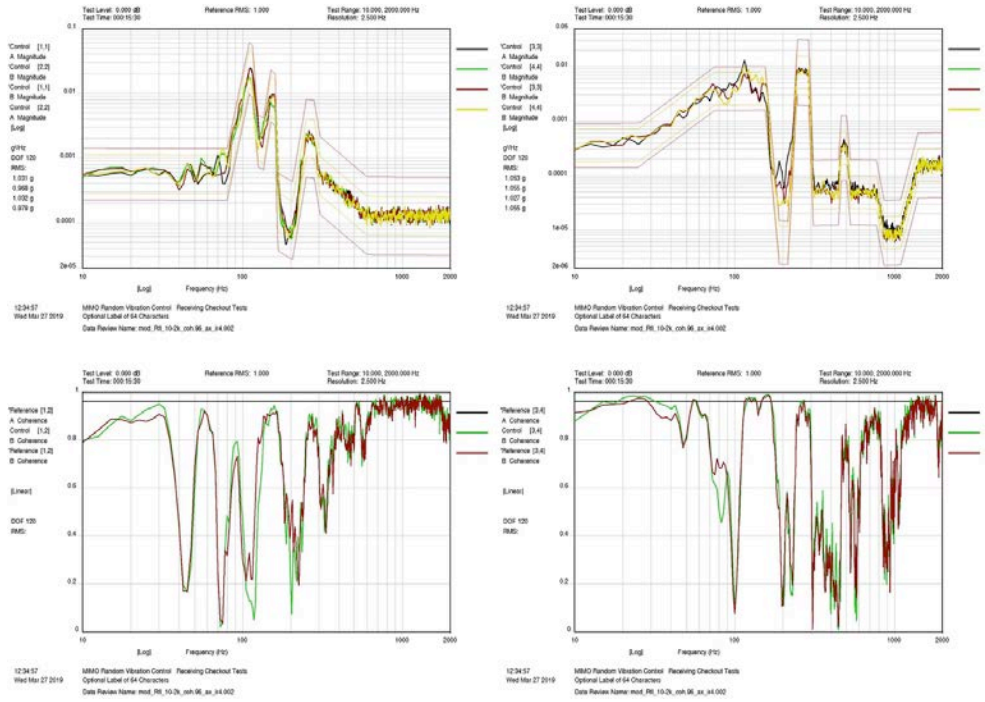

Fig 9: PSD and Coherence Test Results

The top-left plot of Fig. 9 shows the comparison of the PSDs obtained from the two Y-axis control accelerometers for Test A and B, where the Y-1 accelerometer PSD control-response is shown in black for Test A and garnet for Test B; and the Y-2 accelerometer PSD control-response is shown in green for Test A and in yellow for Test B. The PSD comparisons show that Test B's results were largely in tolerance, but that the Test A's

results were slightly worse, being out of tolerance just below 200 Hz in the lower response areas of the Y-axis control-reference PSD profiles. However, the use of the optimal adaptive control was able to minimize the Y-axis difference between Test A and Test B PSDs elsewhere.

However, for the Z-axis PSD results in the upper-right plot of Fig. 9, using the same color-conventions for Test A and Test B, Test A performed significantly worse than Test B. One can see PSD responses outside the test abort tolerance for Z-1 and Z-2 around 115 Hz and 200 Hz for Test A and not for Test B.

The lower two plots shown in Fig. 9, show the response coherence between Y-1 and Y-2 in the lower left and between Z-1 and Z-2 in the lower right for Test B. The pre-specified coherence reference is set to 0.9 and shown as the constant line in black in both the lower left and lower right plots. The two other plots shown in the lower left are the actual coherence control-response in green and the respectively modified control-reference coherence in garnet used for Test B, showing good agreement except slightly worse at the lower frequencies between 20 Hz and 32 Hz, reflecting that the dynamic behavior changed during the test, probably due to the loosening of the couplings as the test progressed.

The lower plots in Fig. 9 shows that the testing system could not support the initially defined high coherence at its various dips around 42, 70, 115, 220, and 330 Hz, due to the rattling and other such non-linearity in the stingers, DUT, and Shakers. The Z-axis performed better, but still with coherence dips at 90, 200, 220, 300, 400, and 500 Hz, again due to the rattling and other such non-linearity. However, the use of the new optimized control-reference SDM improved the coherence control of both axes.

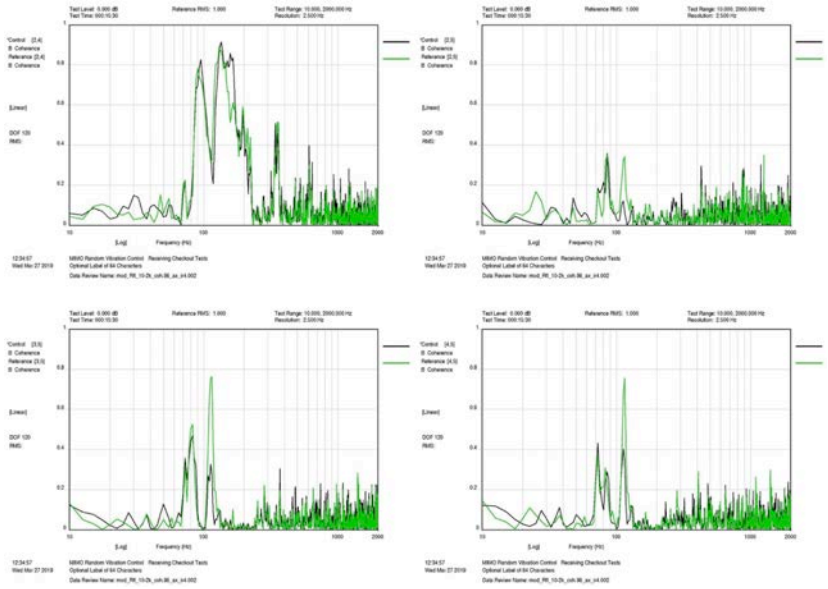

Fig 10: Zero Coherence Test Result

Fig. 10, shows the zero coherence results for dissimilar axis accelerometers for Test B, which had been pre-specified to zero. The control-response coherence between Y-2 and Z-2 accelerometers are shown in the upper-left; the control-response coherence between the

Y-2 accelerometer and the single X accelerometer are shown in the upper-right, both in black and compared to their respective optimal control-reference coherence in green. These plots show excellent agreement with their new reference in both cases. They are both mostly low, except between 75 Hz and 200 Hz in the upper-left and low at most frequencies in the upper-right plots.

The lower set of plots in Fig. 10, respectively show the coherence between Z-1 and the X accelerometers in the lower-left and between Z-2 and X accelerometers in the lower right, again compared to their respective optimal control-reference, with a pre-specified control-reference set to zero, for Test B, using the previous color convention. Again, there was excellent agreement between these control-response coherence values and their respective optimal reference-control coherence spectra. The achieved coherence is low at most frequencies except at the problem 115 Hz, showing independent motion between test axes elsewhere.

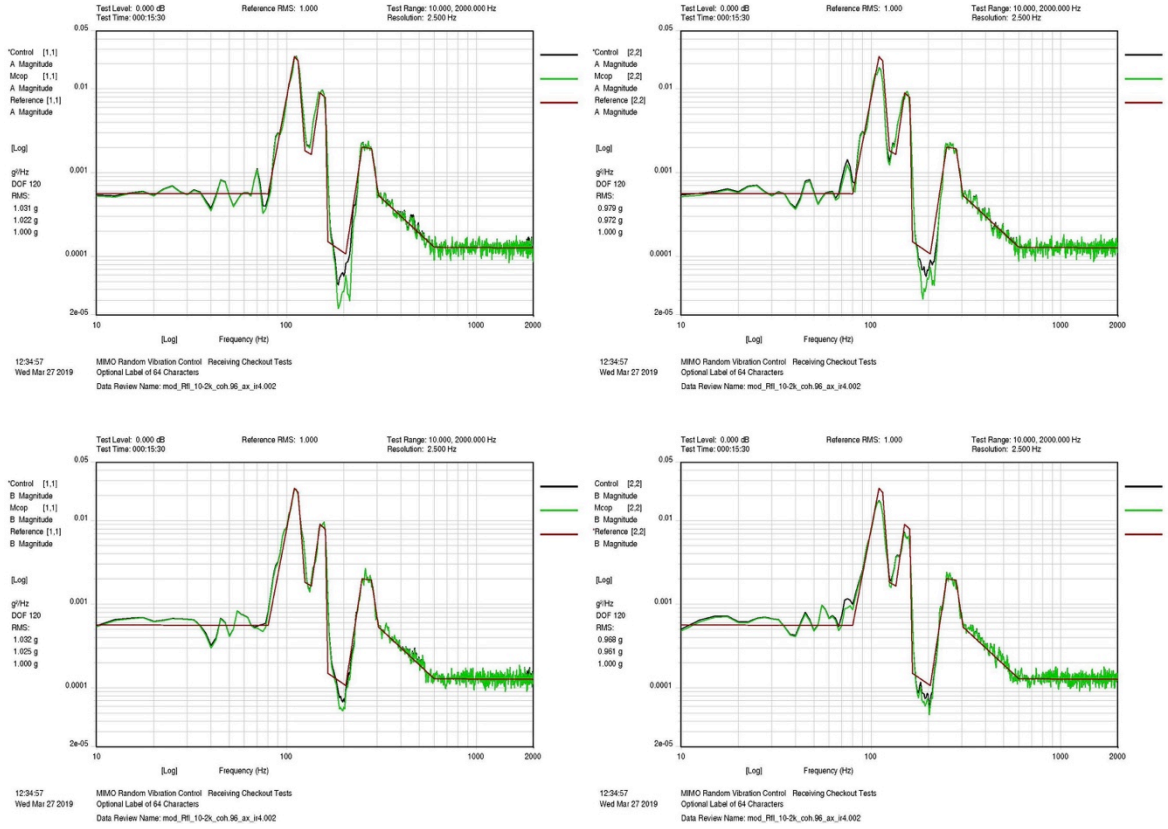

Fig. 11: PSD and MCOP Test Results

Fig. 11, shows the comparison between the control-response PSD in black, their respective MCOP PSD in green, and respective control-reference in garnet for test A on the top row and test B on the bottom row. Results for control accelerometers Y-1 are shown on the left column and Y-2 are shown on the right column. These results are very interesting, because they show better agreement between the two control-response PSDs and their respective MCOP PSDs for Test B than for Test A. This indicates that the use of the new optimized reference produces a more linear response than what was obtained with test A, which uses

the unrealistic pre-specified control-reference that does not account for the limitations of the testing system. Qualitatively, Test B also sounded smoother and quieter, i.e. less rattling, which better explains this result, probably as a result of Test B requiring less drive power as a result of using the new optimized reference and optimal adaptive control.

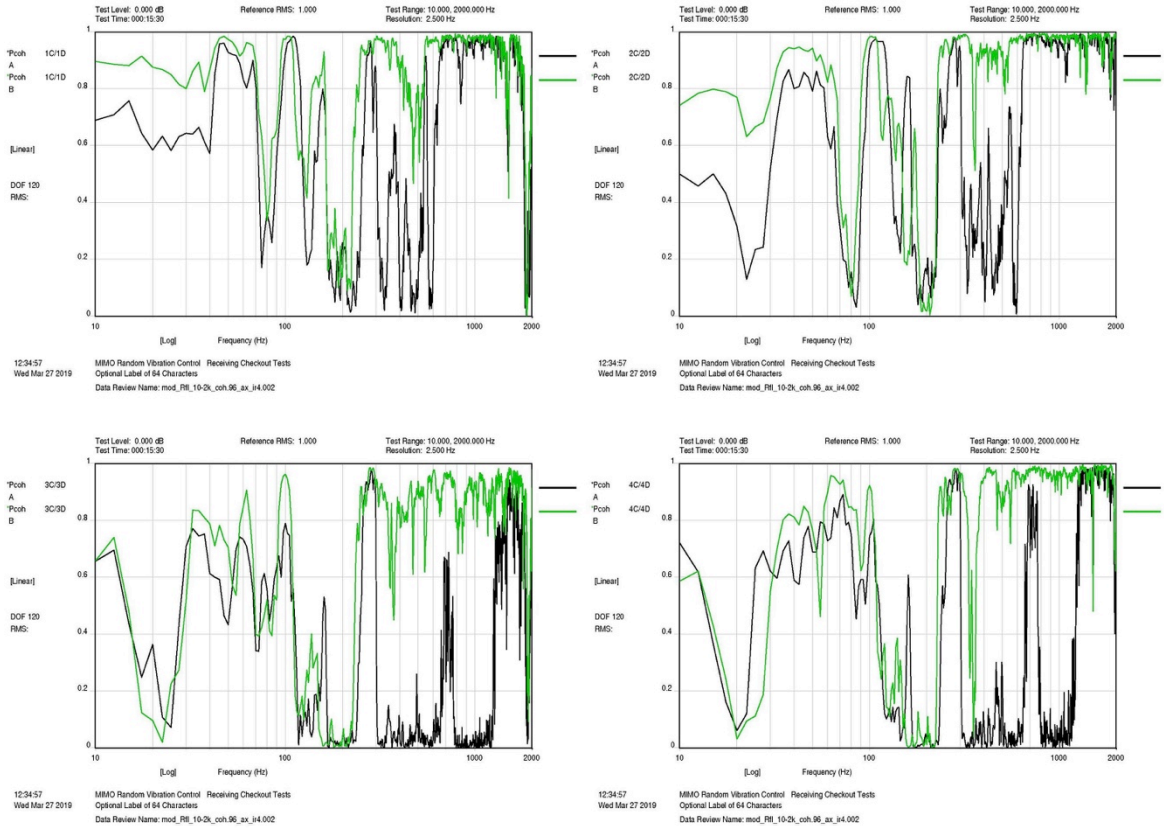

Fig. 12: Partial Coherence Results

The previous Fig. 12, shows the results of measuring the partial coherence between drive Y-1 and control-response Y-1 for Test A in black and Test B in green in the upper left plot and between drive Y-2 and control-response Y-2 in the upper right plot. Notice how much lower the partial coherence results are for Test A than the comparable results for Test B, particularly at the higher frequencies but mostly everywhere except when the control-response exhibits low coherence as expected, given the higher effect of rattling to reduce the partial coherence. This again reflects a higher degree of linear response for the Test B than for Test A, as was shown with the MCOP results, which was also reflected by the smoother quieter sound of Test B than for Test A. As stated previously, this is a consequence from using less drive power to achieve the same test level, which results from using the optimized control-reference that the new method synthesizes.

The lower row of plots in the previous Fig. 12, using the previous color convention, similarly shows partial coherence results between drive Z-1 and control-response Z-1 on its lower left and drive Z-2 and control-response Z-2 on its lower right. The results are very similar to what we saw for the Y-axis comparisons, i.e. the partial coherence is higher for Test B than what it is for Test A for the Z-axis comparisons with the second Z-

axis shakers and control-accelerometers. In this case, the difference is particularly striking for frequencies above 200 Hz. This again shows the Z-axis response is more linear for test B than for test A, which again was reflected as the smoother and quieter sound heard during Test B compared to Test A.

New MIMO Random Test Result Conclusions

- Optimal adaptive control and the use of the new optimized control-reference SDM further reduce control errors in the LMSE sense.
- The use of the new optimized control-reference further reduces the power needed to drive multiple shakers, given the same test level, as compared to a test that does not use the new method.
- New optimal reference SDM synthesis matches the initially specified control-reference SDM in the LMSE sense, while using the testing system and test facility limitations as an optimization constraint, as a function of the definition of the initial control-reference specification and nature of the overall testing system and facility limitations.
- The new method also enables a better match of control-response PSDs to their respective pre-specified reference-control PSDs
- The new method also enables better matching of control-response coherence and phase to their respective new optimized control-reference coherence
- The new method also provides better overall performance for rectangular control
- Improves the linearity of shaker systems as shown by the better match between control-response PSDs and their respective MCOP PSDs.
- Improves the partial coherence between control accelerometers and their respective shakers, again reflecting the improvement of the linearity of the response of an individual control accelerometer due to an individual shaker.

Overall Conclusions

- Advanced adaptive optimal MIMO control produces a closer match between the control-response SDM and the control-reference SDM than other approaches, by performing a control optimization during each iteration of the control loop process.
- New synthesized positive-definite or at least positive semi-definite control-reference SDM, further improves control and avoids the trial-and-error approach used by other least drive methods that don't take into the account its pre-specified off-diagonal elements or the limitations of the overall testing system.
- Use of the optimized control-reference SDM improves uniformity and coherence control via rectangular control, which approximates a pre-determined initial control-reference SDM's off-diagonal elements in the LMSE sense.
- New minimum drive-power control-reference SDM is synthesized by the adaptive optimal control system's inherent optimization methodology and the use of new research results, during an initial low-level pre-test.
- Use of the new control-reference SDM synthesis method further reduces needed drive power and improves control accuracy and excitation system's linearity, by better accounting for limitations in the test system and facility as an optimization constraint.

References:

1. *Hughes et al., "The Development of the Acoustic Design of NASA Glenn Research Center's New Reverberant Acoustic Test Facility," 26th Aerospace Testing Seminar; 29-31 Mar. 2011; Los Angeles, CA*
2. *Jacobsen, Finn; Roisin, Thibaut, "The coherence of reverberant sound fields," Acoustical Society of America. Journal, March 2000*
3. *Kolaini, Ali, et al., "Acoustically Induced Vibration of Structures: Reverberant Vs. Direct Field Acoustic Testing," 25th Aerospace Testing Seminar, October 2009*
4. *Larkin et al., "Status of Direct Field Acoustic Testing," 27th Aerospace Testing Seminar; 16-18 October 2012; Los Angeles, CA*
5. *Larkin, P., Goldstein, R., and Underwood, M., "Direct Field Acoustic Test System and Method," U.S. Patent No. 9,109,972, filed May 27, 2011.*
6. *Maahs, Gordon, "Direct Field Acoustic Test (DFAT) Development and Flight Testing of Radiation Belt Storm Probe (RBSP) Satellites," 27th Aerospace Testing Seminar; 16-18 Oct. 2012; Los Angeles, CA*
7. *Musella et al., "Tackling the target matrix definition in MIMO Random Vibration Control testing," 30th Aerospace Testing Seminar; March 2017; Los Angeles, CA*
8. *Musella et al., "Analyses of drives power reduction techniques for multi-axis random vibration control tests," Mechanical Systems and Signal Processing, January 2020*
9. *National Aeronautics and Space Administration, "NASA TECHNICAL HANDBOOK: NASA-HDBK-7010—2016-02-01," NASA, February 1, 2016.*
10. *Smallwood, David 0.,"Random Vibration Testing of a Single Test Item with a Multiple Input Control System," IES Proceedings, 1982*
11. *Smallwood, David 0.,"Multiple Shaker Random Vibration Control-An Update," IES Proceedings, 1999*
12. *Smallwood, David O., "Multiple-Input Multiple-Output (MIMO) linear systems extreme inputs/outputs," Shock and Vibration, Vol. 14, No. 2, (2007) pp 107-132.*
13. *Smallwood, David O., "The challenges of multiple input vibration testing and analysis," Presented at the Experimental and Analytical joint HOCWOG, Los Alamos National Labs, May 20, 2013, https://www.osti.gov/servlets/purl/1095931*
14. *Underwood, Marcos A., "Adaptive Control Method and System for MultiExciter Swept-Sine Testing," U.S. Patent No. 5,299,459, April 5, 1994.*
15. *Underwood et al., "A Review of Multi-axis Multi-exciter Vibration Technology," Sound and Vibration, April 1996*
16. *Underwood, Marcos A., "Adaptive Control Method and System for Transient Waveform Testing," U.S. Patent No. 5,517,426, May 14, 1996.*
17. *Underwood, Marcos A., "Applications of Computers to Shock and Vibration," Shock and Vibration Handbook, 5th Ed., Chapter 27, Edited by Harris, C. M., and Piersol, A. G., McGraw-Hill, New York, 2001*
18. *Underwood, M., and Keller, T., "Rectangular Control of Multi-Shaker Systems; Theory and some practical results," Journal and Proceedings - Institute of Environmental Sciences and Technology, April 2003*
19. *Underwood, M. and Keller, T., "Applying Coordinate Transformations to Multi Degree of Freedom Shaker Control," Proceedings of the 74th Shock and Vibration Symposium, October, 2003, San Diego, California.*

20. *Underwood, M., and Keller, T., "Understanding and using the Spectral Density Matrix," 76th Shock and Vibration Symposium Proceedings, Oct. 2005, Destin, Fl.*
21. *Underwood, M. and Keller, T., "Using the Spectral Density Matrix to Determine Ordinary, Partial, and Multiple Coherence," Proceedings of the 77th Shock and Vibration Symposium, October 2006, Monterrey, CA.*
22. *Underwood, M., and Hale, M., "MIMO Testing Methodologies," Proceedings of the 79th Shock and Vibration Symposium, October 2008; Orlando, Fl.*
23. *Underwood, Marcos A., "Digital Control Systems for Vibration Testing Machines," Shock and Vibration Handbook, 6th ed., Chapter 26, Edited by Piersol et al., T. L., McGraw-Hill, New York, 2009*
24. *Underwood, M., Keller, T., and Ayres, R., "Some Aspects of using Measured Data as the Basis of a Multi-Exciter Vibration Test," IMAC-XXVIII Proceedings, Feb. 1–4, 2010, Jacksonville, Florida*
25. *Underwood, M. and Keller, T.; "Applications of MIMO Coherent Output Power Analysis to Multi-Shaker Testing"; Presented at the 85th Shock and Vibration Symposium, October 26 – 29, 2014, Reston, VA.*
26. *Underwood, Marcos A., "Applications of Digital Control Techniques to High Level Acoustic Testing," 31st Aerospace Testing Seminar; Oct. 2018; Los Angeles, CA*
27. *Underwood, Marcos A., "Applications of MIMO Digital Adaptive Control to High Level Acoustic Testing," 26th International Congress on Sound & Vibration; July 2019; Montreal, Canada*
28. *Underwood, Marcos A., "Comparisons of the Structural Response of a Test Article Excited by DFAT Diffuse and Non-Diffuse Acoustic Fields," 91st Shock and Vibration Symposium, September 19 – 23, 2021, Orlando, Fl.*
29. *Underwood, M. Keller, T., Ayres, R., "Multi-Shaker Control: A Review of the Evolving State-of-the-Art," Sound & Vibration, August 2017*

Biography:

Marcos A. Underwood has a Ph.D. in Electrical Engineering, with specialization in control and communication systems, and a Masters in Mathematics, both from the University of California in Los Angeles. He also has a Masters in Structural Engineering from San Jose State University. His Bachelors, in Mathematics and Physics, is from the California State University in Los Angeles. Dr. Underwood worked with Philco-Ford Aeronutronic, Rockwell International Space Div. on the Space Shuttle project, and Hughes Helicopters on Structural Dynamics and Acoustics, early in his career, developing the use of digital vibration and acoustic control and analysis systems. Later, he also worked with SD, GenRad, STI, and again with SD as their systems architect, designer of their vibration and acoustic control and analysis systems over the years. Afterwards, he held the positions Chief Engineer, V.P of Engineering, and Chief Scientist at STI and SD. During the three phases, he developed some of the fundamental digital technology now used for vibration and acoustic control and analysis. He has been involved in the use, design, and development of digital control and analysis systems for vibration and acoustics for almost 50 years and holds many key patents in the field. He has authored many publications, is a Fellow of the IEST, and the chair of the recommended practices IEST-RP-DTE 022 working group committee on Multi-Shaker Testing and Control. He currently works, from his consulting firm Tu'tuli Enterprises, with MSI DFAT as their Chief Scientist.